Atom-molecule conversion with particle losses

B. Cui, L. C. Wang, and X. X. Yi
School of Physics and Optoelectronic Technology, Dalian University of Technology, Dalian 116024, China
(Received 28 February 2011; published 12 January 2012)

Based on the mean-field approximation and the phase-space analysis, we study the dynamics of atom-molecule conversion systems subject to particle losses. Starting from the many-body dynamics described by a master equation, an effective nonlinear Schrödinger equation is introduced. The classical phase space is then specified and classified by fixed points. The boundaries, which separate different dynamical regimes, have been established and discussed. The effect of particle loss on the conversion efficiency and the self-trapping is explored. By numerically solving the master equation, we show that the mean-field approximation is a good approach to study the dynamics of this atom-molecule conversion system.

DOI: 10.1103/PhysRevA.85.013618 PACS number(s): 03.75.−b, 07.60.Ly

I. INTRODUCTION

Association of ultracold atoms into molecules is currently an active topic in the field of ultracold quantum physics; it attracts much attention due to its applications ranging from the production of molecular Bose-Einstein condensates to the search for permanent electric dipole moments (see, for example, [1–13]). By applying a time-varying magnetic field in the vicinity of Feshbach resonance, a pair of atoms can be bound into a diatomic molecule [14,15]; this conversion can be described by the Gross-Pitaevskii (GP) equations within the mean-field theory (MFT) [16–21], which reduces the full many-body problem into a set of coupled nonlinear Schrödinger equations and maps the complicated many-body dynamics into the dynamics of a two-mode system. Earlier study shows that the nonlinearity, which arises from the atom-atom and molecule-molecule couplings, plays an important role in the dynamics of the system [17]; for example, four distinct regimes, each having different feature in dynamics, can be classified, and accordingly, the bifurcation of the fixed points in the classical phase space [17,21] can be identified.

Every quantum system is inevitably coupled to its surrounding environment. For Bose-Einstein condensates [22–27], the thermal atoms or molecules may play the role of the surrounding environment. Description of decoherence by fully including the quantum effects requires sophisticated theoretical studies; it is complicated and difficult to solve. Fortunately, the standard approach in quantum optics can reduce the complexity, and in fact, it has been widely used in the study of Bose-Einstein condensates in recent years [28–33]. For an atom-molecule conversion system, we then ask, how does the decoherence affect the dynamics of the atom-molecule conversion system? What are the fixed points in this atom-conversion system? How do these fixed points behave? We will answer these questions in this paper.

In this paper, we will focus on the effect of decoherence in the atom-molecule conversion system. The decoherence may arise from inelastic collision between condensate and noncondensate atoms or molecules in the system. These inelastic collisions may lead to dissipation (or particle loss) and dephasing for the system. Here we consider only the dissipative effect due to particle loss and neglect the dephasing that conserves the particle number. Under the mean-field approximation, an effective non-Hermitian Gross-Pitaevskii equation is derived. Bifurcation of the fixed points divides the parameter space into different dynamical regimes, and boundaries that separate these regimes are changed by the decoherence. By calculating the Jacobian matrix, we find that a sudden transition in the fixed point from elliptic point to attractor or repeller happens with a nonzero decoherence rate. The atom-molecule conversion efficiency and the self-trapping for the system are also studied.

This paper is organized as follows. In Sec. II, we introduce the model and transform the master equation into a nonlinear Schrödinger equation. In Sec. III, we define different regimes by the fixed points and study the dynamics in these regimes. In Sec. IV, we investigate the effect of particle loss on the conversion efficiency. In Sec. V, we shed light on the self-trapping, taking the decoherence into account, and an explanation for the predicted features is also given. Finally, we conclude our results in Sec. VI.

II. MODEL

Based on the two-mode approximation, the Hamiltonian that includes the atom-atom collision U_{aa}, atom-molecule conversion with rate V, and molecule-molecule couplings U_{bb} takes the following form [17,18]:

$$H = \mu_a \hat{a}^\dagger \hat{a} + \mu_b \hat{b}^\dagger \hat{b} + U_{aa} \hat{a}^\dagger \hat{a}^\dagger \hat{a}\hat{a} + U_{bb} \hat{b}^\dagger \hat{b}^\dagger \hat{b}\hat{b} + U_{ab} \hat{a}^\dagger \hat{a} \hat{b}^\dagger \hat{b} + V(\hat{a}^\dagger \hat{a}^\dagger \hat{b} + \hat{b}^\dagger \hat{a}\hat{a}). \quad (1)$$

The master equation [34] that takes the particle loss into account can be written as [22]

$$\dot{\rho} = -i[\hat{H}, \rho] - \frac{\Gamma_a}{2}(\hat{a}^\dagger \hat{a}\rho + \rho \hat{a}^\dagger \hat{a} - 2\hat{a}\rho\hat{a}^\dagger) - \frac{\Gamma_b}{2}(\hat{b}^\dagger \hat{b}\rho + \rho \hat{b}^\dagger \hat{b} - 2\hat{b}\rho\hat{b}^\dagger), \quad (2)$$

where Γ_a and Γ_b represent decoherence rates for atoms and molecules, respectively. In the mean-field approximation, the quantum fluctuation is neglected, and the operators $\hat{a}$ and $\hat{b}$ can be replaced with c numbers $a = |a|e^{i\theta_a}$ and $b = |b|e^{i\theta_b}$, respectively. With these considerations, the master equation (2) can be cast into the following nonlinear Schrödinger equation:

$$i\frac{d}{dt}\begin{pmatrix} a \\ b \end{pmatrix} = H\begin{pmatrix} a \\ b \end{pmatrix}, \quad (3)$$

$$H = \begin{pmatrix} R - Uz - \frac{i}{2}\Gamma_a & 2Va^* \\ Va & -2R + 2Uz - \frac{i}{2}\Gamma_b \end{pmatrix}, \quad (4)$$

with $z = |a|^2 - 2|b|^2$ denoting the number difference of atoms in the atom and molecule modes. $U = \frac{1}{4}U_{ab} - \frac{1}{2}U_{aa} - \frac{1}{8}U_{bb}$ represents the coupling strength, and V is the conversion rate. $R = \frac{1}{4}(2\mu_a - \mu_b + 2U_{aa} - \frac{1}{2}U_{bb})$ denotes the energy difference between the two modes, which can be effectively adjusted by a time-varying external field [18,19]. Units are chosen such that $\hbar = 1$ throughout this paper.

The Hilbert space for such an atom–diatomic-molecule conversion system is spanned by a set of Bloch vectors. Under the mean-field approximation, the Bloch vectors can be defined by [20]

$$\vec{h} = \{2\sqrt{2}\mathrm{Re}[(a^*)^2 b], 2\sqrt{2}\mathrm{Im}[(a^*)^2 b], |a|^2 - 2|b|^2\}. \quad (5)$$

With the normalization condition $|a|^2 + 2|b|^2 = 1$ (for the case without decoherence), the Bloch sphere is a teardrop-shaped surface (as shown in Fig. 3).

To analyze the dissipative dynamics of the system in its classical phase space, we define relative phase θ, particle number n, and normalized population difference S as

$$\theta = 2\theta_a - \theta_b, \quad (6)$$

$$n = 2|b|^2 + |a|^2, \quad (7)$$

$$S = \frac{z}{n}. \quad (8)$$

Inserting these definitions into Eq. (3), a set of evolution equations is obtained:

$$\dot{S} = -2\Omega(1+S)\sqrt{1-S}\sin\theta - \Gamma_-(1-S^2), \quad (9)$$

$$\dot{\theta} = 4CS - 4R - \Omega\frac{1-3S}{\sqrt{1-S}}\cos\theta, \quad (10)$$

$$\dot{n} = -(\Gamma_+ + \Gamma_- S)n, \quad (11)$$

where $\Gamma_+ = \frac{1}{2}(\Gamma_a + \Gamma_b)$ and $\Gamma_- = \frac{1}{2}(\Gamma_a - \Gamma_b)$ have been defined as representing the total and relative decoherence rates for the two modes, respectively. $C = Un$ and $\Omega = V\sqrt{n}$ represent a rescaled coupling strength and conversion rate, respectively. The particle number $n(t)$ is initially normalized to $n(0) = 1$, and the Block vectors $\vec{h}$ were normalized by $n(t)$ in the rest of paper. Without decoherence, i.e., $\Gamma_a = \Gamma_b = 0$, the dynamics of the system can be described by a classical Hamiltonian,

$$H = 2\Omega(1+S)\sqrt{1-S}\cos\theta - 2CS^2 + 4RS, \quad (12)$$

where θ and S are conjugate variables. By this classical Hamiltonian, the authors of Refs. [17,21] have found that the bifurcation of the fixed points falls into four regimes in the parameter space (see Fig. 1). A natural question arises: how does the decoherence affect these regimes and the dynamics? We will explore this question in the next section.

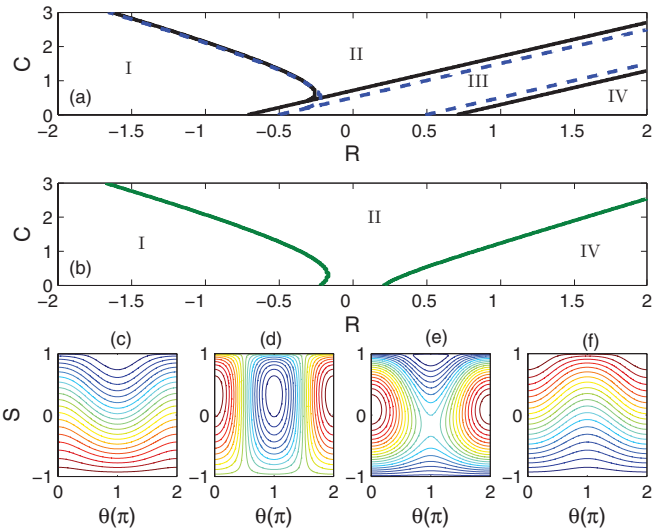

FIG. 1. (Color online) Parameter space spanned by nonlinearity C and energy difference R. $\Omega = 1$. Here and in the following, C, Ω, and R are rescaled in units of V, and t is in units of $1/V$; hence all parameters are dimensionless. (a) Different regimes are separated by boundary lines, where black solid lines represent the case for $\Gamma_- = 0$, while blue dashed lines denote the case for $\Gamma_- = -1$. (b) Green solid lines denote the boundary lines for $\Gamma_- = -1.5$. Γ_+ has no effect on the distribution of fixed points according to Eqs. (14) and (15), but it affects the lifetime of metastable process [see Eq. (18)]. The classical phase space for regimes (c) I, (d) II, (e) III, and (f) IV is shown for the case without decoherence.

III. FOUR DYNAMICAL REGIMES WITH DECOHERENCE

We divide this section into two parts. First, we study the dynamics with fixed C and Ω; i.e., $n(t)$ is treated as a constant [28,32]. Because the particle number $n(t)$, in fact, is time dependent and decreases with time, this discussion is valid for a short time scale, within which the change of $n(t)$ does not destroy the phase-space structure and cannot induce transitions between different regimes; this is similar to the scenario discussed in Refs. [28,32], and the dynamics can be seen as a metastable process. Second, we take the change of $n(t)$ into account and explore the transition between different regimes.

A. Slow and small change of $n(t)$

In this section, we consider a scenario where $n(t)$ changes slowly and the change of $n(t)$ is small. In this case, $n(t)$, C, and Ω can be treated as constants. When $n(t)$ in Eq. (11) changes slowly with respect to $S(t)$ and $\theta(t)$ in Eqs. (9) and (10), S and θ can reach a "fixed point" for each $n(t)$. The following analogy well characterizes the situation under study: a moving twister characterized by a spiraling funnel-shaped wind current connected to a large cumulus or cumulonimbus cloud. Although the center of the twister moves, the air can keep rotating around the center. The fixed point in the next section is similar to the center of the twister; it moves but it still can be found as a metastable process. Mathematically, this is the case when the change rate $\delta = \Gamma_+ + \Gamma_- S$ of n in Eq. (11) is very small. Further consideration shows that $\delta \ll 1$ equals to $\Gamma_b \gg \Gamma_a$ and $S(0) \approx 1$, or $\Gamma_a \gg \Gamma_b$ and $S(0) \approx -1$.

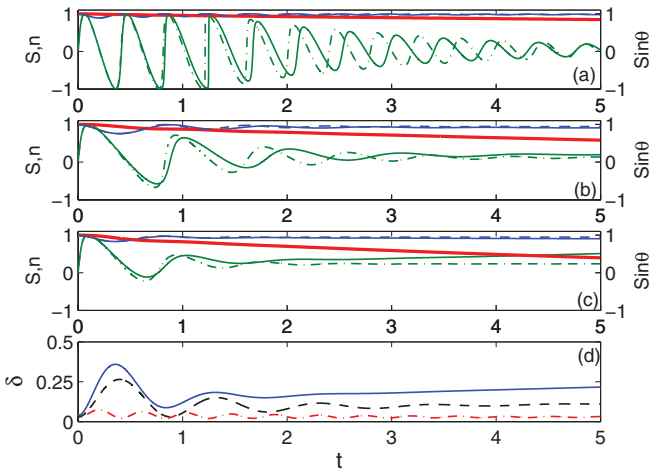

FIG. 2. (Color online) (a), (b), and (c) Parameters $n(t)$, $S(t)$, and $\theta(t)$ as a function of time. The red thick solid line and the blue (top) and green (bottom) solid lines represent the time evolution of n, S, and $\sin\theta$, respectively. These results are from numerically solving Eqs. (9)–(11). These results are compared with that from solving only Eqs. (9) and (10) with $n(t)$ keeping its initial value, $n(t) = 1$. Blue dashed and green dash-dotted lines are for S and $\sin\theta$ in this case. The parameters chosen are $R = 0$, $\Omega(0) = 1$, $S(0) = 0.99$, and $\theta(0) = 0$ for (a), (b), and (c). $C(0) = 4$, $\Gamma_- = -0.49$, $\Gamma_+ = 0.51$ for (a). $C(0) = 2$, $\Gamma_- = -0.99$, $\Gamma_+ = 1.01$ for (b). $C(0) = 2$, $\Gamma_- = -1.99$, $\Gamma_+ = 2.01$ for (c). (d) The time evolution of δ corresponding to (a), (b), and (c) is shown by the red dash-dotted line, black dashed line, and blue solid line, respectively.

The former corresponds to an attractor near $S = 1$, while the latter corresponds to an attractor near $S = -1$. Because the lifetime for a molecular condensate is much shorter than that of an atomic condensate in experiments [35,36], we numerically check the first case and plot the results in Fig. 2. Namely, we plot the time evolution for population difference S and relative phase θ by numerically solving Eqs. (9)–(11) and compare the solution to the results by only solving Eqs. (9) and (10) with $n(t) = 1$. We find that, for small $\Gamma_+ \simeq \Gamma_-$, the two results for $S(t)$ and $\theta(t)$ coincide. As $\Gamma_+ \simeq \Gamma_-$ increases, the consistent time becomes shorter, but it can still last a long time. Meanwhile, time evolution of δ remains smaller (less than 1) under the condition we considered.

With these notations, the fixed points of the system are defined by

$$\dot{S} = \dot{\theta} = 0. \tag{13}$$

By this definition, we can calculate the fixed points and find that one of the fixed points is $S = -1, \theta = \arccos(-\frac{\sqrt{2}(C+R)}{\Omega})$, while the other fixed points are determined by

$$\begin{aligned}&(9\Gamma_-^2 + 64C^2)S^3 - (\Gamma_-^2 - 4\Omega^2 + 64R^2)\\ &-(15\Gamma_-^2 - 36\Omega^2 + 64C^2 + 128CR)S^2\\ &-(24\Omega^2 - 7\Gamma_-^2 - 64R^2 - 128CR)S = 0\end{aligned} \tag{14}$$

and

$$\sin\theta = -\frac{\Gamma_-}{2\Omega}\sqrt{1-S}. \tag{15}$$

By a Jacobian matrix defined as

$$J = \begin{pmatrix} \partial\dot{S}/\partial S & \partial\dot{S}/\partial\theta \\ \partial\dot{\theta}/\partial S & \partial\dot{\theta}/\partial\theta \end{pmatrix}, \tag{16}$$

we can study the stability of the fixed points and classify the phase space as in the literature [33,37,38]. All parameters used here are realizable with recent technologies. To be specific, the lifetimes for atomic and molecular condensates can be on the order of 10 s [35] and 1 s [36], which is consistent with dissipation rates in our paper. The ratio between the nonlinear strength C and the conversion rate Ω is adjustable with the help of Feshbach resonance [15], for example, the MIT experiment parameters with ^{23}Na condensate [39], giving the mean density of the condensate $n \sim 10^{15}$ cm^{-3} and $C/\Omega = 0.36$.

In Ref. [17], without decoherence effects, the parameter space was divided into four regimes by the feature of fixed points. Here, using Eq. (16), we redivide the regimes by taking the decoherence into account (see Figs. 1, 3, and 4). Boundaries that separate different regimes are determined by numerically solving Eqs. (14) and (15). Note that the fixed points on the boundary behave like the fixed points in the regime labeled by a smaller number (for example, the boundary that separates regimes I and II belongs to regime I).

Figure 1(c) shows the Poincaré section of the classical Hamiltonian for regime I. The only fixed point is located near the border of the phase space ($S = 1$), and the dynamics of the

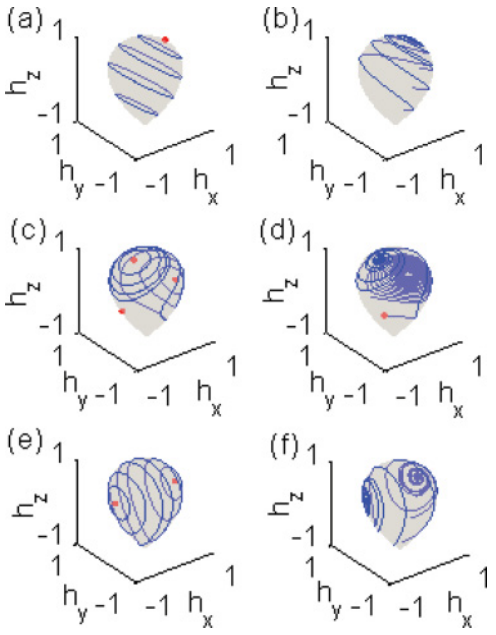

FIG. 3. (Color online) Mean-field dynamics on the Bloch sphere for cases (left) without and (right) with decoherence. The north pole and south pole of the sphere correspond to the pure atomic condensate and the pure molecular condensate, respectively. Red spots and the center of the vortex denote the location of the fixed points. Blue solid lines represent the trajectories for the time evolution of the system. Parameters chosen are $R = 1$, $\Omega = 1$, $C = 0$ for (a) and (b), $R = 0$, $\Omega = 1$, $C = 2$ for (c) and (d), and $R = 0$, $\Omega = 1$, $C = 0$ for (e) and (f). (a), (c), and (e) are for the case without decoherence (i.e., $\Gamma_+ = \Gamma_- = 0$), while (b), (d), and (f) depict the case with decoherence ($\Gamma_+ = 1$ and $\Gamma_- = -1$).

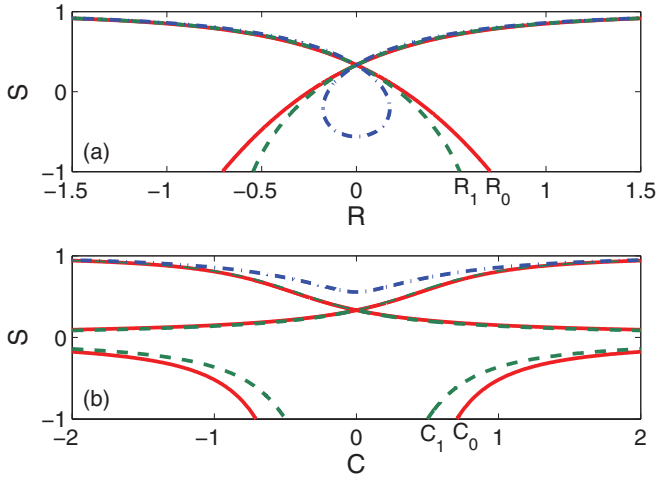

FIG. 4. (Color online) (a) Locations of fixed points vs energy difference R. Parameters chosen are $C = 0$, $\Omega = 1$, and $\Gamma_- = 0, 0.9, 1.6$ for red solid line, green dashed line, and blue dash-dotted line, respectively. (b) Locations of fixed points vs interaction strength C. Parameters chosen are $R = 0$, $\Omega = 1$, and $\Gamma_- = 0, -0.5, -1.5$ for red solid line, green dashed line, and blue dash-dotted line, respectively. This figure is a result of Eq. (14).

system is localized. When taking the decoherence into account, the fixed point near $S = 1$ turns into an attractor, and Figs. 3(a) and 3(b) show trajectories on the teardrop-shaped Bloch sphere. The dynamics of the system becomes delocalized due to the appearance of such an attractor.

By changing the energy difference R and the nonlinearity C [see Fig. 1(a)], the system can go across the boundary into regime II, and the fixed point in regime I bifurcates into two elliptic points and a hyperbolic one, as Fig. 1(d) shows. Regime II shares similar features with the self-trapping in the two-mode Bose-Hubbard model [40,41]. With a negative relative decoherence rate, both of the two elliptic fixed points transit to attractors in this regime [see Figs. 3(c) and 3(d)], while the locations of the stable attractors are just slightly changed due to the decoherence [see Fig. 4(b)].

Figure 1(e) illustrates the Poincaré section of the classical Hamiltonian for regime III without decoherence. In this regime, large-amplitude oscillations around the elliptic fixed can be observed; see Fig. 3(e). With $C = 0$ and $R = 0$, the location of the fixed points in this regime can be derived analytically:

$$(S,\theta) = \begin{pmatrix} \frac{1}{3},\pi + \arcsin\left(\frac{\Gamma_-}{\sqrt{6}\Omega}\right) \\ \frac{1}{3},2\pi - \arcsin\left(\frac{\Gamma_-}{\sqrt{6}\Omega}\right) \end{pmatrix}, \tag{17}$$

where we assume the relative decoherence rate positive and the relative phase was restricted in $\theta \in [0,2\pi]$. From Eq. (17), we find that the relative phase between the two fixed points decreases, and the fixed points becomes asymmetric due to the decoherence effect [see Fig. 3(f)]. As the relative decoherence rate increases, the area of regime III is compressed [see blue dashed line in Fig. 1(a)]. The two boundaries coincide, and regime III vanishes [see dash-dotted line in Fig. 4(a)]; when the relative decoherence rate is larger than a threshold ($\Gamma_- > \sqrt{2}\Omega$), a hyperbolic fixed point arises from the bottom of the phase space [see dash-dotted line in Fig. 4(a)]. The boundary that separates regimes III and IV is shifted due to decoherence. This boundary shift can be explained as a threshold decrease in the energy difference R [denoted by R_0 and R_1 in Fig. 4(a)], which is a evidence for the bifurcation of fixed points in classical phase space.

The dynamics in regime IV behaves similarly to that in regime I. The elliptic fixed point turns into an attractor due to the negative relative decoherence rate, and the dynamics in this regime then becomes delocalized [see Figs. 3(a) and 3(b)].

Next, we focus on the changes of the fixed points; such a change in classical phase space is fundamental for a non-Hermitian Bose-Hubbard system [28,32,33]. However, we find that, in the atom-molecule conversion system, the change differs from the Bose-Hubbard model in two respects. First, the type of the fixed point (e.g., a repeller or an attractor) is determined by the the sign of relative decoherence rate Γ_- and the location of the fixed point S. If Γ_- and S are different in sign, i.e., one of them is positive while the other is negative, the original elliptic fixed point transits into a stable attractor. Otherwise, the original fixed point turns into an unstable repeller. Second, the transition is *sudden*. In other words, the transition happens provided the decoherence rate is not zero. This is different from the decoherence effect on Bose-Einstein condensates in a double-well potential; namely, there exists a critical value for the decoherence rate [28]. In the atom-molecule conversion system, the transition happens once the decoherence exists, regardless of how small the decoherence is. This feature reflects not only the

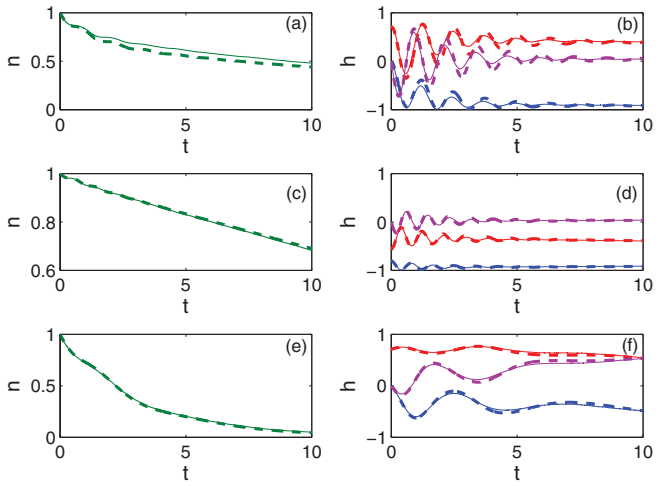

FIG. 5. (Color online) Comparison of the results under the mean-field approximation (thin solid line) with the results by solving the master equation (2) (thick dashed line). (left) n denotes the normalized particle number. (right) $\vec{h}$ stands for the Bloch vector. The three components of $\vec{h}$, h_x, h_y, and h_z, are plotted in red, purple, and blue, respectively. The lower line is for h_z, h_x and h_y differ at the initial value. (a) and (b) describe regimes I and IV with initial conditions $\vec{h}(t=0) = (0.707,0,0)$, $R = 1$, $\Omega(0) = 1$, $C(0) = 0$, $\Gamma_+ = 0.5$, and $\Gamma_- = -0.5$. (c) and (d) depict regime II with $\vec{h}(t=0) = (-0.57,0,-0.8)$, $R = 0$, $\Omega(0) = 1$, $C(0) = 2$, $\Gamma_+ = 0.5$, and $\Gamma_- = -0.5$. (e) and (f) depict regime III with $\vec{h}(t=0) = (0.707,0,0)$, $R = 0$, $\Omega(0) = 1$, $C(0) = 0$, $\Gamma_+ = 0.5$, and $\Gamma_- = -0.5$. Initially, the total number of particles is 100, and all the particle are in the atomic condensate.

metastable behavior of the open many-particle system, but also the sensitivity of the atom-molecule conversion system to the particle loss.

To show the validity of the mean-field theory, we numerically solve the master equation (2) by the Monte Carlo wave-function method. The results are presented in Fig. 5. From Fig. 5 we find that the mean-field approximation is a good approach to study the dynamics of the atom-molecule conversion system.

B. Transition between different regimes induced by the change of $n(t)$

The decreasing of $n(t)$ leads to decreasing $C(t)$ and $\Omega(t)$. For a small change of $C(t)$ and $\Omega(t)$ [the change is due to the change of $n(t)$], the number of fixed points and the feature of the fixed points do not change; however, for a large change of $C(t)$ and $\Omega(t)$, this is no longer true. In this section, we study the effect of the time-dependent interaction strength $C(t)$ and conversion strength $\Omega(t)$ on the dynamics of the system. Different regimes are distinguished by the number of fixed points in the phase space. When $C(t)$ and $\Omega(t)$ change with time, the number and locations of fixed points [roots of Eqs. (14) and (15)] change as well, which causes the transition between different regimes. To learn where and when the transition happens, we have numerically solved Eqs. (14) and (15), and we plot the fixed points S as a function of $n(t)$ in Fig. 6. When the system is initially prepared in regime II (three fixed points in phase space) [see Figs. 6(a) and 6(b)], it transits to regime I (one fixed point) when n decreases to a critical value (see the red squares in Fig. 6). The number of fixed points can be counted as the number of lines in Fig. 6. From Figs. 6(a) and 6(b) or Figs. 6(c) and 6(d), we can find that the critical value of n increases with the decoherence rate. We cannot compare the critical value of n in Figs. 6(a) and 6(c) [or in Figs. 6(b) and 6(d)] because the other parameters are different in these two plots. This observation can be made by comparing the squares in Figs. 6(a) and 6(b). This observation shows that the regime transition happens earlier for strong particle loss. The same conclusion can be drawn by observing the red squares in Figs. 6(c) and 6(d). When the system starts in regime III, it transits to regime II before it transits to I, which means two transitions exist in the dynamics [see squares in Figs. 6(c) and 6(d)]. In Figs. 6(c) and 6(d), the line located at $S \approx 0.3$ denotes two fixed points that share the same S but different θ. Besides numerically solving the equations, we can give part of the analytic explanation for the transition as well. For simplicity, we restrict our discussion to the symmetric case ($R = 0$). By observing the roots of Eq. (14), we find that, with weak dissipation [$\Gamma_- < 2\Omega(t)$], the number of the fixed points remains unchanged (there are three fixed points), and the system will stay in regime II. However, for a large dissipation rate [$\Gamma_- > 2\Omega(t)$], the number of real roots for Eq. (14) decreases to one or two, depending on the value of the interaction strength $C(t)$. If $C(t) > F(\Omega,\Gamma_-)$ [where F is a function of $\Omega(t)$ and Γ_-, which is complicated and not given here], there is only one fixed point; otherwise, two fixed points exist in the phase space. This indicates the transition from regime II to regime I or regime III.

Due to the moving of fixed points and the transition between different regimes, there are no true fixed points for the system. So the dynamics of the system is a metastable process, and the transition between different fixed points is unavoidable. If the dynamics begins with a small dissipation rate, the system initially converges to the attractive fixed point near its initial state (see Fig. 7). However, as $n(t)$ decreases, the conversion

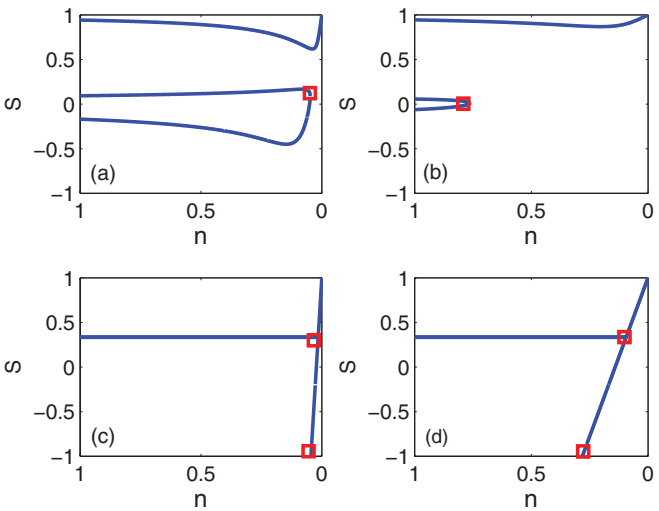

FIG. 6. (Color online) Fixed points of population difference S as a function of particle number n. The parameters chosen are $C(0) = 2$, $R = 0$, and $\Omega(0) = 1$ for (a) and (b) and $C(0) = 0$, $R = 0$, and $\Omega(0) = 1$ for (c) and (d). Dissipation rates are $\Gamma_- = -0.45, -1.75, -0.2, -0.75$ for (a), (b) (c), and (d), respectively. Red squares denote the points where the regimes change.

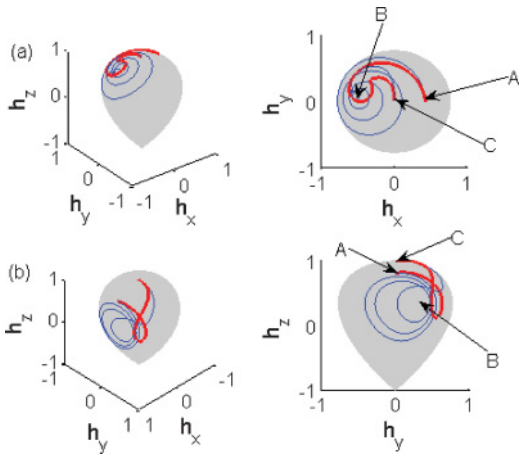

FIG. 7. (Color online) Metastable process for the atom-molecule conversion system with decoherence. (a) Metastable process in regime II. The parameters chosen are $R = 0$, $C(0) = 2$, $\Omega(0) = 1$. $\Gamma_- = -1.75$, $\Gamma_+ = 2.25$ for the thick red line and $\Gamma_- = -0.45$, $\Gamma_+ = 0.55$ for the thin blue line. (b) Metastable process in regime III. The parameters chosen are $R = 0$, $C = 0$, $\Omega(0) = 1$. $\Gamma_- = -0.2$, $\Gamma_+ = 0.3$ for the thin blue line, and $\Gamma_- = -0.75$ and $\Gamma_+ = 1.25$ for the thick red line. Spot A denotes the initial state of the system in the phase space, spot B represents the attractor that the system initially converges to, namely, the steady state with constant particle number [which is a root of Eq. (14) with constant n], and spot C denotes the (resulting) steady state of the system. The left and right plots of both (a) and (b) are the same but show the feature from different angles.

strength Ω and coupling strength C get smaller and smaller, and at an instance of time $\Omega(t)$ is smaller than a threshold $[\Omega(t) < 0.5\Gamma_-]$, the original fixed point disappears, and the system has to converge to a new fixed point (see thin blue lines in Fig. 7). This effect can be understood as a manifestation of metastable behavior of the many-particle system. If the dissipation rate is large, the metastable process becomes much shorter (see thick red lines in Fig. 7). In addition, comparing Figs. 6 and 7, we can learn the exact regime transition route in Fig. 7, and the value of the critical point n can denote the strength of such a metastable process (Figs. 6 and 7 share the same parameters). The final state of the system will be the fixed point at $S = 1,\theta = 0$ or $S = -1,\theta = 0$ (top or bottom of the Bloch sphere), which depends on the sign of Γ_-. This can be understood by examining Eqs. (9) and (10), which become $\dot{S} = -\Gamma_-(1 - S^2)$ and $\dot{\theta} = 0$ when $n(t)$ decreases to nearly zero. When Γ_- is negative, the only fixed point left is $S = 1$ (see Fig. 6). By calculating the eigenvalues of Eq. (16), we find that negative Γ_- corresponds to the attractor $S = 1$, whereas positive Γ_- leads to the attractor $S = -1$.

To measure the length of such a metastable process, we define a lifetime T by $\Omega(T) = 0.5\Gamma_-$ for the metastable process. This is based on the analytical results that the number of fixed points will not change until the condition $\Omega(T) = 0.5\Gamma_-$ is satisfied. We now derive an approximate lifetime for the metastable process with a small dissipation rate $[\Gamma_- < 2\Omega(0)]$. From Eq. (11), we can get the particle number $n(T)$ at time T. Inserting $n(T)$ into $\Omega(T) = 0.5\Gamma_-$, the lifetime for the metastable process is given by

$$T = \frac{2\ln 2\Omega(0) - 2\ln|\Gamma_-|}{\Gamma_+ + \Gamma_- S(0)}, \tag{18}$$

where $S(0)$ is the location of the fixed point. The approximation here relies on the average of $S(t)$ in the metastable process, which is taken approximately to be $S(0)$ here. We find that T could be an approximate lifetime for most cases; this can be found by comparing T with numerical results.

IV. CONVERSION EFFICIENCY FOR MOLECULAR CONDENSATE

In experiments, the association of ultracold atoms into diatomic molecules can be achieved by applying a time-dependent magnetic field in the vicinity of a Feshbach resonance, which corresponds to the change between different regimes (I → III → IV) in the parameter space (see Fig. 1). To examine the effect of decoherence on the conversion process, we define the conversion efficiency, relative efficiency, and sweeping rate of the external field as follows:

$$W = \frac{|b(T)|^2}{n(T)}, \tag{19}$$

$$M = \frac{W(\Gamma_-,\Gamma_+) - W(0)}{W(0)}, \tag{20}$$

$$\beta = \dot{R}, \tag{21}$$

where T denotes the final time for the conversion and $W(\Gamma_-,\Gamma_+)$ and $W(0)$ denote the conversion efficiency with and without decoherence, respectively. M describes the relative increases or decreases of the efficiency with and without decoherence. By adjusting the external magnetic field [18], R can be linearly manipulated to cross the Feshbach resonance point ($R = \beta t - R_0, R_0 = \beta T, t \in [0,2T]$) until the system relaxes into a steady state. The conversion efficiency with decoherence has been calculated with the same parameters, and a pure atomic mode $[|a(0)|^2 = 1]$ at $t = 0$ was chosen for this plot, see Fig. 8.

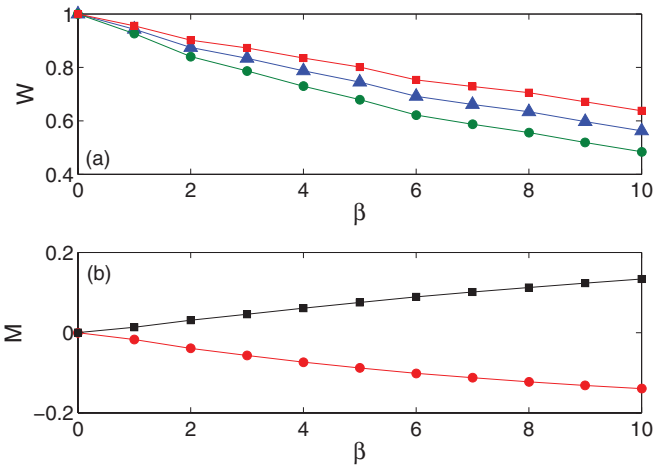

FIG. 8. (Color online) (a) Conversion efficiency W and (b) relative efficiency M as a function of the sweeping rate β. Here β is rescaled in units of V^2. The parameters chosen are $C(0) = 0$ and $\Omega(0) = 1$ for both (a) and (b). The dissipation rates chosen are $\Gamma_- = \Gamma_+ = 0$ for the blue line with triangles in (a), $\Gamma_- = -\Gamma_+ = -0.1$ for the green line with circles in (a), and the red line with circles in (b); $\Gamma_- = \Gamma_+ = 0.1$ for the red line with squares in (a) and the black line with squares in (b).

The results of W show that conversion efficiency increases with a positive relative decoherence rate, while a negative relative decoherence rate decreases the conversion efficiency (see Fig. 8). This can be interpreted by the appearance of an attractor or repeller in the phase space. That is, for a negative relative decoherence rate, the elliptic fixed points near the atomic mode would turn into an attractor, and the atoms are repelled from the molecular mode [see Figs. 3(b) and 3(f)]. The conversion process is depressed by such an attractor, and the conversion efficiency decreases. Similarly, a positive relative decoherence rate will increase the conversion efficiency.

V. TUNNELING AND SELF-TRAPPING

In this section, we investigate the effect of particle loss on the dynamics of the system; the atoms may oscillate between atomic and molecular modes (corresponding to regime III), and they can also be trapped in one of the modes (corresponding to regime II in the parameter space).

In regime III, the atoms oscillate between the atomic mode and the molecular mode [see Fig. 3(e)]. When the relative decoherence rate is positive, the fixed point transits from being elliptic to being a repeller, and the amplitude of the oscillation is then increased [see dash-dotted line in Fig. 9(a)]. However, for a negative relative decoherence rate, the oscillation is

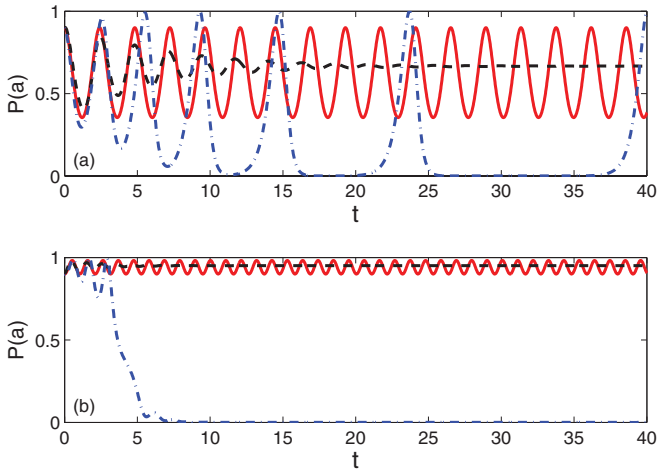

FIG. 9. (Color online) Time evolution for the population of the atomic mode $P(a) = |a(t)|^2$ under different decoherence rates: $\Gamma_+ = \Gamma_- = 0$ for the red solid line, $\Gamma_+ = 0.5$ and $\Gamma_- = -0.5$ for the black dashed line, and $\Gamma_+ = 0.5$ and $\Gamma_- = 0.5$ for the blue dash-dotted line in both (a) and (b). The parameters chosen are $\Omega(0) = 1$, $R = 0$ for both (a) and (b) and $C(0) = 0$ for (a) and $C(0) = 1.5$ for (b). The initial population for atoms is $|a(0)|^2 = 0.9$, and the population for the atomic mode is normalized by the particle number n.

compressed since the elliptic fixed point suddenly transits into an attractor [see dashed line in Fig. 9(a)].

As C increases, the dynamics of the system turns into the self-trapping regime, which belongs to regime II in Fig. 1(a). We find that the threshold of the coupling constant is decreased by the decoherence; i.e., the decoherence supports the self-trapping [denoted by C_0 and C_1 in Fig. 4(b)]. With a negative relative decoherence rate, the fixed point near the atomic mode transits into an attractor. The self-trapping in the atomic mode remains [see black dashed line in Fig. 9(b)]. When the relative decoherence rate is positive, which indicates a repeller in the phase space, the self-trapping in the atomic mode is ruined because the atoms are repelled and converted into molecules, as the dash-dotted line shows in Fig. 9(b).

VI. CONCLUSION

In summary, we have investigated the effect of particle loss on the dynamics of the atom-molecule conversion system. Within the mean-field approximation, the classical phase space is specified, and the fixed points are calculated. Due to the bifurcation of the fixed points in the phase space, the parameter space can be divided into different regimes. We find that the boundary that separates different regimes is changed by the decoherence. A sudden transition of the fixed points from elliptic to attractor or repeller happens. Such a transition not only reflects the metastable behavior of the system but also characterizes the phase-space structure of the atom-molecule conversion system. The effect of decoherence on the conversion efficiency and the self-trapping is also explored with the mean-field approximation.

ACKNOWLEDGMENTS

This work is supported by NSF of China under Grants No. 61078011, No. 10935010, and No. 11175032, the Open Research Fund of State Key Laboratory of Precision Spectroscopy, East China Normal University, and the National Research Foundation and Ministry of Education, Singapore, under academic research Grant No. WBS: R-710-000-008-271.

[1] D. J. Heinzen, R. Wynar, P. D. Drummond, and K. V. Kheruntsyan, Phys. Rev. Lett. **84**, 5029 (2000).
[2] E. Donley, N. Claussen, S. Thompson, and C. Wieman, Nature (London) **417**, 529 (2002).
[3] J. J. Hudson, B. E. Sauer, M. R. Tarbutt, and E. A. Hinds, Phys. Rev. Lett. **89**, 023003 (2002).
[4] M. Greiner, C. A. Regal, and D. S. Jin, Nature (London) **426**, 537 (2003).
[5] S. Jochim, M. Bartenstein, A. Altmeyer, G. Hendl, S. Riedl, C. Chin, J. Hecker Denschlag, and R. Grimm, Science **302**, 2101 (2003).
[6] M. W. Zwierlein, C. A. Stan, C. H. Schunck, S. M. F. Raupach, S. Gupta, Z. Hadzibabic, and W. Ketterle, Phys. Rev. Lett. **91**, 250401 (2003).
[7] A. P. Hines, R. H. McKenzie, and G. J. Milburn, Phys. Rev. A **67**, 013609 (2003).
[8] C. A. Regal, M. Greiner, and D. S. Jin, Phys. Rev. Lett. **92**, 040403 (2004).
[9] P. Naidon, E. Tiesinga, and P. S. Julienne, Phys. Rev. Lett. **100**, 093001 (2008).
[10] M. Junker, D. Dries, C. Welford, J. Hitchcock, Y. P. Chen, and R. G. Hulet, Phys. Rev. Lett. **101**, 060406 (2008).
[11] H. Jing, Y. G. Deng, and W. P. Zhang, Phys. Rev. A **80**, 025601 (2009).
[12] J. Qian, W. P. Zhang, and H. Y. Ling, Phys. Rev. A **81**, 013632 (2010).
[13] W. Zhang, Y. Huang, T. Xie, G.-R. Wang, and S.-L. Cong, Phys. Rev. A **82**, 063411 (2010).
[14] E. Timmermans *et al.*, Phys. Rep. **315**, 199 (1999).
[15] T. Köhler, K. Góral, and P. S. Julienne, Rev. Mod. Phys. **78**, 1311 (2006).
[16] A. Vardi, V. A. Yurovsky, and J. R. Anglin, Phys. Rev. A **64**, 063611 (2001).
[17] G. Santos, A. P. Tonel, A. Foerster, and J. Links, Phys. Rev. A **73**, 023609 (2006).
[18] J. Li, D.-F. Ye, C. Ma, L.-B. Fu, and J. Liu, Phys. Rev. A **79**, 025602 (2009).
[19] B. Liu, L.-B. Fu, and J. Liu, Phys. Rev. A **81**, 013602 (2010).
[20] L.-B. Fu and J. Liu, Ann. Phys. **325**, 2425 (2010).
[21] G. Santos, A. Foerster, J. Links, E. Mattei, and S. R. Dahmen, Phys. Rev. A **81**, 063621 (2010).
[22] J. Anglin, Phys. Rev. Lett. **79**, 6 (1997).
[23] J. Ruostekoski and D. F. Walls, Phys. Rev. A **58**, R50 (1998).
[24] A. Vardi and J. R. Anglin, Phys. Rev. Lett. **86**, 568 (2001).

[25] J. R. Anglin and A. Vardi, Phys. Rev. A **64**, 013605 (2001).
[26] W. Wang, L. B. Fu, and X. X. Yi, Phys. Rev. A **75**, 045601 (2007).
[27] N. Syassen, D. M. Bauer, M. Lettner, T. Volz, D. Dietze, J. J. García-Ripoll, J. I. Cirac, G. Rempe, and S. Dürr, Science **320**, 1329 (2008).
[28] F. Trimborn, D. Witthaut, and S. Wimberger, J. Phys. B **41**, 171001 (2008).
[29] D. Witthaut, F. Trimborn, and S. Wimberger, Phys. Rev. Lett. **101**, 200402 (2008).
[30] D. Witthaut, F. Trimborn, and S. Wimberger, Phys. Rev. A **79**, 033621 (2009).
[31] V. S. Shchesnovich and V. V. Konotop, Phys. Rev. A **81**, 053611 (2010).
[32] E. M. Graefe, H. J. Korsch, and A. E. Niederle, Phys. Rev. Lett. **101**, 150408 (2008).
[33] E. M. Graefe, H. J. Korsch, and A. E. Niederle, Phys. Rev. A **82**, 013629 (2010).
[34] C. W. Gardiner and P. Zoller, *Quantum Noise* (Springer, Berlin, 2004).
[35] D. M. Stamper-Kurn, M. R. Andrews, A. P. Chikkatur, S. Inouye, H.-J. Miesner, J. Stenger, and W. Ketterle, Phys. Rev. Lett. **80**, 2027 (1998).
[36] G. Thalhammer, K. Winkler, F. Lang, S. Schmid, R. Grimm, and J. Hecker Denschlag, Phys. Rev. Lett. **96**, 050402 (2006); K. Winkler, F. Lang, G. Thalhammer, P. v. d. Straten, R. Grimm, and J. Hecker Denschlag, *ibid.* **98**, 043201 (2007); R. Wynar, R. S. Freeland, D. J. Han, C. Ryu, and D. J. Heinzen, Science **287**, 1016 (2000).
[37] S. H. Strogatz, *Nonlinear Dynamics and Chaos* (Addison-Wesley, New York, 1994).
[38] W. E. Boyce and R. C. Diprima, *Elementary Differential Equations and Boundary Value Problems* (Wiley, New York, 1997).
[39] J. Stenger, S. Inouye, M. R. Andrews, H.-J. Miesner, D. M. Stamper-Kurn, and W. Ketterle, Phys. Rev. Lett. **82**, 2422 (1999).
[40] A. Smerzi, S. Fantoni, S. Giovanazzi, and S. R. Shenoy, Phys. Rev. Lett. **79**, 4950 (1997).
[41] M. Albiez, R. Gati, J. Fölling, S. Hunsmann, M. Cristiani, and M. K. Oberthaler, Phys. Rev. Lett. **95**, 010402 (2005).